HIGH PRESSURE HYDROGEN TANK RUPTURE: BLAST WAVE AND FIREBALL

Kim, W, Shentsov, V. Makarov, D. and Molkov, V.
HySAFER, Ulster University, Shore Road, Newtownabbey, BT37 0QB, UK,
w.kim@ulster.ac.uk

ABSTRACT

In the present study, the phenomena of blast wave and fireball generated by high pressure (35 MPa) hydrogen tank (72 *l*) rupture have been investigated numerically. The realizable k-ε turbulence model was applied. The simulation of the combustion process is based on the eddy dissipation model coupled with the one step chemical reaction mechanism. Simulation results are compared with experimental data from a stand-alone hydrogen fuel tank rapture following a bonfire test. The model allows the study of the interaction between combustion process and blast wave propagation. Simulation results (blast wave overpressure, fireball shape and size) follow the trends observed in the experiment.

1.0 INTRODUCTION

Mainstream solutions for onboard hydrogen storage in automotive applications use high-pressure GH2 tanks made of carbon fiber reinforced plastic (CFRP) with plastic as a liner material (so called type 4 tank) or aluminium (type 3 tank). Various regulations and standards require bonfire testing of onboard tanks to ensure that the tank maintains structural integrity in fire and hydrogen is safely released using a temperature activated pressure relief device (TPRD). However, tank rupture remains a potential hazard associated with car fires due to localized transient heating or TPRD failure. Understanding the consequences of tank rupture in a realistic environment and acquiring the ability to predict tank rupture hazards is a challenging safety engineering problem important for design of hydrogen storage and its infrastructure.

The fire exposure tests of Type 3 and Type 4 hydrogen fuel tanks without PRDs were conducted by Weyandt, N. et. al. [1-3]. The stand-alone Type 4 tank had had length 0.84m, diameter 0.41 m, 72.4 *l* volume, 35 MPa storage pressure, and was installed 0.20m above ground. The tank ruptured catastrophically after 6 min 27 sec of exposure to a propane bonfire. Experimental measurements demonstrated the blast pressures 300 kPa, 83 kPa and 41 kPa at 1.9 m, 4.2 m and 6.5 m respectively, and the maximum diameter of the fireball about 7.7 m. Tank fragment projectiles were found at distances of 34 m to 82 m. In the test of Type 3 tank which was installed under a car, blast wave overpressure was ranging from 140 kPa at 1.2 m to 12 kPa at 15m and the maximum fireball diameter was 24m. The projectiles were discovered at distances up to 107 m. Such experimental results indicate that tank rupture may have devastating consequences, causing damage to life and property at substantial distances from tank location.

In view of the above considerations, the objectives of this study are to investigate the blast wave and fireball phenomena which develop in a realistic environment and to reproduce in numerical simulations the experimental results [1-3].

2.0 NUMERICAL MODEL

The governing equations included three dimensional Favre-averaged compressible conservation equations for mass, momentum, energy and species:

$$\frac{\partial \rho}{\partial t} + \frac{\partial}{\partial x_j}\left(\rho u_i\right) = 0, \tag{1}$$

$$\frac{\partial \bar{\rho} u_i}{\partial t} + \frac{\partial}{\partial x_j}\left(\bar{\rho} u_i u_j\right) = -\frac{\partial \bar{p}}{\partial x_i} + \frac{\partial}{\partial x_j}\left(\mu + \mu_t\right)\left(\frac{\partial u_i}{\partial x_j} + \frac{\partial u_j}{\partial x_i} - \frac{2}{3}\frac{\partial u_k}{\partial x_k}\delta_{ij}\right) + \rho g_i, \tag{2}$$

$$\begin{aligned}&\frac{\partial}{\partial t}\left(\bar{\rho} E\right) + \frac{\partial}{\partial x_j}\left(u_j(\bar{\rho} E + p)\right)\\ &= \frac{\partial}{\partial x_j}\left[\left(k + \frac{\mu_t c_p}{\mathrm{Pr}_t}\right)\frac{\partial T}{\partial x_j} - \sum_m h_m\left(-\left(\rho D_{H_2} + \frac{\mu_t}{Sc_t}\right)\frac{\partial Y_{H_2}}{\partial x_j}\right) + u_i\left(\mu + \mu_t\right)\left(\frac{\partial u_i}{\partial x_j} + \frac{\partial u_j}{\partial x_i} - \frac{2}{3}\frac{\partial u_k}{\partial x_k}\delta_{ij}\right)\right] + S_E,\end{aligned} \tag{3}$$

$$\frac{\partial \bar{\rho} Y_{H_2}}{\partial t} + \frac{\partial}{\partial x_j}\left(\bar{\rho} u_j Y_{H_2}\right) = \frac{\partial}{\partial x_j}\left[\left(\rho D_{H_2} + \frac{\mu_t}{Sc_t}\right)\frac{\partial Y_{H_2}}{\partial x_j}\right] + S_{H_2}, \tag{4}$$

where ρ is the density, t is the time, x_i, x_j, x_k are Cartesian coordinates, u_i, u_j, u_k are the velocity components, p is the pressure, g_i is the gravity acceleration in i direction, μ_t is the turbulent dynamic viscosity, δ_{ij} is Kronecker symbol, E is the total energy, T is the temperature, Y_{H2} is the hydrogen mass fraction, c_p is the specific heat at constant pressure, Sc_t is the turbulent Schmidt number, Pr_t is the turbulent Prandtl number, D_{H2} is the hydrogen molecular diffusivity, S_E, S_{H2} are the source terms in energy conservation and hydrogen conservation equations due to combustion [4].

The turbulence is accounted using the realizable k - ε model in this simulation [5]. The transport equation of turbulence kinetic energy, k and its rate of dissipation ε are as follows:

$$\frac{\partial}{\partial t}\left(\rho k\right) + \frac{\partial}{\partial x_j}\left(\rho k u_j\right) = \frac{\partial}{\partial x_j}\left[\left(\mu + \frac{\mu_t}{\sigma_k}\right)\frac{\partial k}{\partial x_j}\right] + G_k + G_b - \rho\varepsilon - Y_M, \tag{5}$$

$$\frac{\partial}{\partial t}\left(\rho \varepsilon\right) + \frac{\partial}{\partial x_j}\left(\rho \varepsilon u_j\right) = \frac{\partial}{\partial x_j}\left[\left(\mu + \frac{\mu_t}{\sigma_\varepsilon}\right)\frac{\partial \varepsilon}{\partial x_j}\right] + \rho C_1 S\varepsilon - \rho C_2 \frac{\varepsilon^2}{k + \sqrt{\nu\varepsilon}} + C_{1\varepsilon}\frac{\varepsilon}{k}C_{3\varepsilon}G_b, \tag{6}$$

where $C_1 = \max\left[0.43, \frac{\eta}{\eta + 5}\right], \eta = S\frac{k}{\varepsilon}, S = \sqrt{2S_{ij}S_{ij}}$.

In these equations, G_k is the generation of turbulent kinetic energy by the mean velocity gradients. G_b is the generation of turbulent kinetic energy by the buoyancy, Y_M is the contribution of the fluctuating dilatation in compressible turbulence flow to the dissipation rate, C_2, $C_{1\varepsilon}$ and $C_{3\varepsilon}$ are constants, σ_k and σ_ε are the turbulent Prandtl numbers for each k and ε.

The Eddy Dissipation model based on the work of Magnussen and Hjertager [6] is employed to model combustion and turbulence-chemistry interaction. The net rate of production of species i in reaction r, $R_{i,r}$, is given by

$$R_{i,r} = \nu'_{i,r} M_{w,i} A\rho \frac{\varepsilon}{k} \min R\left(\frac{Y_R}{\nu'_{R,r} M_{w,R}}\right), \tag{7}$$

$$R_{i,r} = \nu'_{i,r} M_{w,i} AB\rho \frac{\varepsilon}{k} \frac{\sum_P Y_P}{\sum_j^N \nu''_{j,r} M_{w,j}}, \tag{8}$$

where $\nu'_{i,r}$, $\nu''_{j,r}$ are the stoichiometric coefficients for reactants *i* and *j* due to reaction, $M_{w,i}$, $M_{w,j}$ are the molecular weights of species *i* and *j*, Y_p and Y_R are the mass fractions of the product and the reactant respectively, A=4.0 and B=0.5 are empirical constants. The chemical reaction is controlled by the large-eddy mixing time scale, and combustion occurs when k/ε >0. In this simulation, the one-step chemical reaction mechanism of hydrogen combustion in the air is applied, and the model is therefore unable to predict kinetics of intermediate species.

3.0 NUMERICAL DETAILS

The computational domain is shown in Figure 1. The domain was a 100 m diameter hemisphere designed to account for both the blast wave and the fireball propagation. The hydrogen tank area was meshed using a tetrahedral mesh with the CV size changing from 0.010 to 0.017 m. Domain for the surrounding tank area was a 2 m diameter hemisphere and it was discretized the CV size changing from 0.01 to 0.1 m. The calculation domain for the fireball propagation was a 10 m diameter hemisphere and was meshed using a tetrahedral mesh with the control volume (CV) size changing from 0.015 to 0.1m. The rest of the domain was meshed using CVs size 0.1-1.5 m. The total number of CVs was 944,868. In the described simulations the initial hydrogen mass fraction in the tank was set to Y_{H2}=1.0 and initial pressure to p=35 MPa. The ground was modelled as a non-slip impermeable adiabatic boundary. A far-field non-reflective boundary was set at the interface with ambient atmosphere. ANSYS Fluent software was used as a CFD platform [7]. Coupled compressible solver with explicit time stepping was used in the simulations with Courant–Friedrichs–Lewy number equal 0.8. Convective terms were discretized using second order upwind scheme and diffusive terms – using second order central difference scheme. Tank rupture was modelled as instantaneous disappearance of the tank wall.

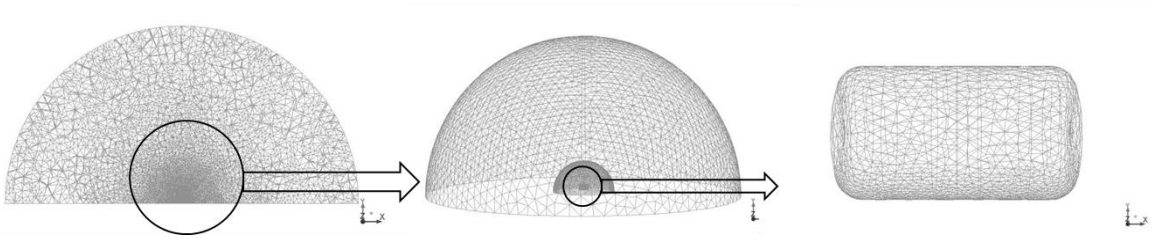

a) b) c)

Figure 1. Computational domain and numerical mesh: a) central cross section, b) side view of the domain boundary, fireball resolution area, and tank location, c) tank boundary mesh

4.0 RESULTS AND DISCUSSIONS

4.1 Blast wave

Figure 2 shows the pressure wave propagation in the area surrounding tank due to the rupture of the high pressure hydrogen tank at different times. After the tank rupture, the high pressure is instantly released and the blast wave reflects off the ground and the reflected wave catches up with the head blast wave. The pressure decays rapidly due to spherical expansion. The reproduced blast wave propagation is plausible and follows expected physical behavior – wave shape is generally hemispherical, with slightly larger overpressure formed closer to the ground (instances t=5.1×10^{-4}, 9.1×10^{-4} and 1.5×10^{-3} s), probably, due to the fact that the tank is not located in the centre of computational hemisphere, but 0.1 m above ground. Figure 2 (instance t=3.1×10^{-4} s) also shows the formation of secondary pressure wave, which, being reflected from the ground, provided the largest overpressure of about 47 bar. This wave continues to travel back and forth between ground and

hydrogen-air interface, providing unexpectedly high pressures in the focal point on the ground, e.g. about 5 bar overpressure at the moment t=2.1×10^{-3} s, which apparently give rise to the next pressure wave quickly running through hydrogen to catch-up with the initial blast wave propagating through the air with slower velocity.

The variations of the temperature and the velocity in the surrounding atmosphere due to the rupture of the high pressure hydrogen tank are shown in Fig. 3 and Fig. 4 respectively. Again, temperature profile is generally physical. Air temperature increases in the area of adiabatic compression by the blast wave. Hydrogen, on the other hand, adiabatically expands and temperature there falls below ambient one. Combustion contribution to temperature rise is negligible during blast wave propagation through the domain even though the combustion model is formally engaged from the start of simulations. As a result the largest temperatures are observed in the area of pressure wave reflection close to the ground. Thus, the maximum temperature on the ground increases till 1750 K at t=3.1×10^{-4} s. It is interesting, that though high-temperature profile, coinciding with blast wave propagation, is generally hemispherical, the low temperature area of expanding hydrogen is not hemispherical. The low temperature area has preferential propagation direction along the longitudinal and transverse tank axes and the authors believe this is the result of cylindrical shape of high-pressure hydrogen charge.

Velocity profile reflects the development of the blast wave and hydrogen expansion. Initially coupled blast and hydrogen expansion waves provide a single high-velocity profile, visible in Figure 2 at t=7.5×10^{-5} and t=3.1×10^{-4} s. Already at t=5.1×10^{-4} s velocity profile is decoupled showing clearly two waves – one corresponding to blast wave and the other – to expanding hydrogen. The maximum velocity magnitude 1780m/s is observed at the moment corresponding to the maximum blast wave pressure, i.e. at t=7.5×10^{-4} s, then the maximum velocity decreases as the blast wave propagates.

In Figure 5 the calculated overpressure is compared with the experimental results of the stand-alone tank versus the distances from the tank. The calculated overpressure at 1.9 m agrees with the experimental value. However, the calculated values at 4.2 m and 6.5m are underestimated. One reason for the difference between the experiments and the calculations is maybe that the materials of the tank were neglected in this calculation, although the cylindrical tank had a high-density polyethylene inner liner, a carbon fiber structural layer, and a protective fiberglass outer layer in the bonfire test. Another possibility is that the internal pressure in the experimental tests might be increased by exposure to the bonfire, which total heat release rate was equal 370 kW. The results from a previous numerical study on the heat transfer of 70 MPa hydrogen composite tanks in the bonfire test [8] demonstrated that the internal hydrogen pressure in the middle of the tank increased from 70 MPa to 76 MPa during 600 s of fire exposure, which could be another reason for the discrepancy between experimental and numerical results in this study.

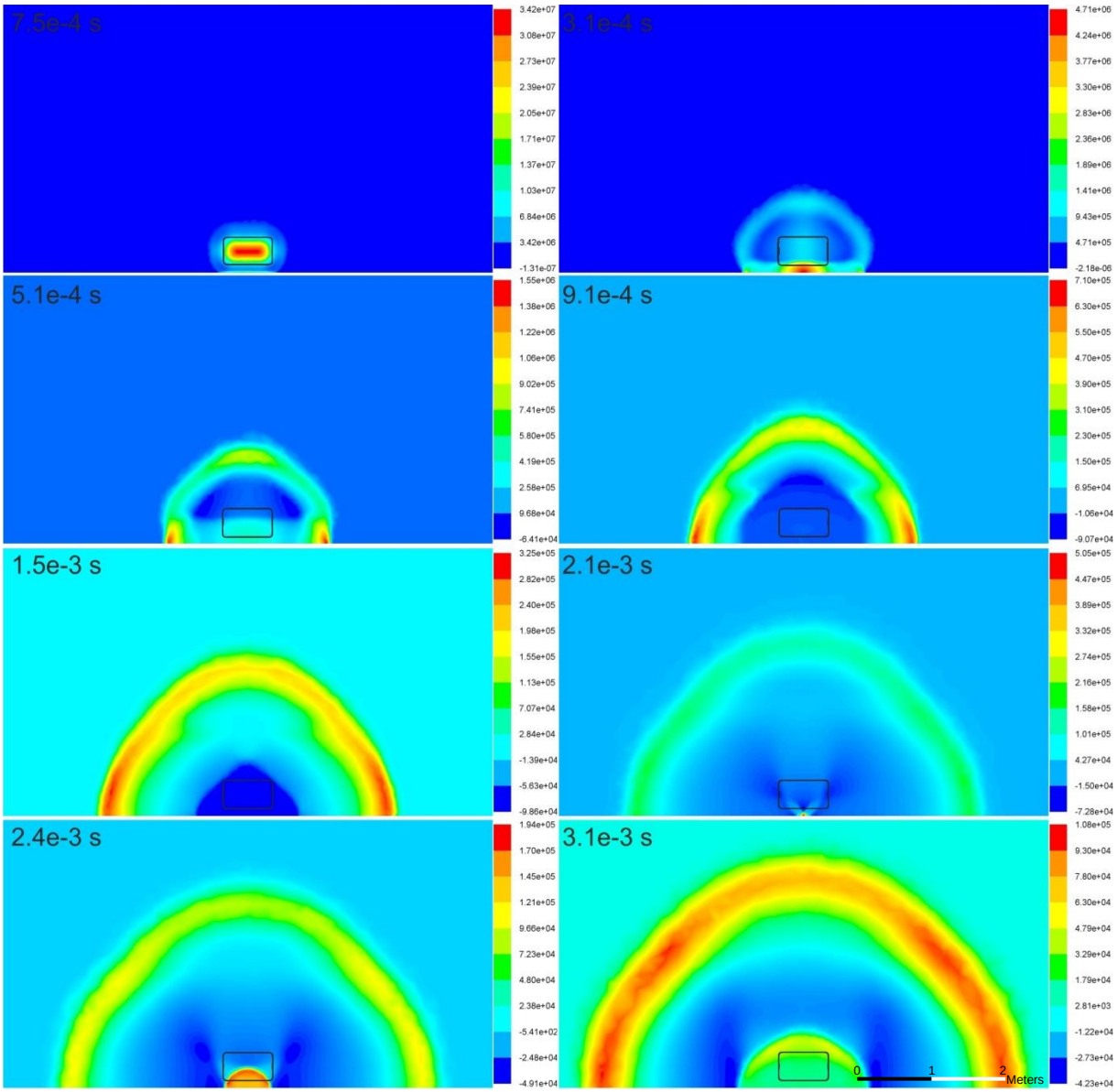

Figure 2. Pressure wave in the surroundings of the tank due to the rupture of the high pressure hydrogen tank

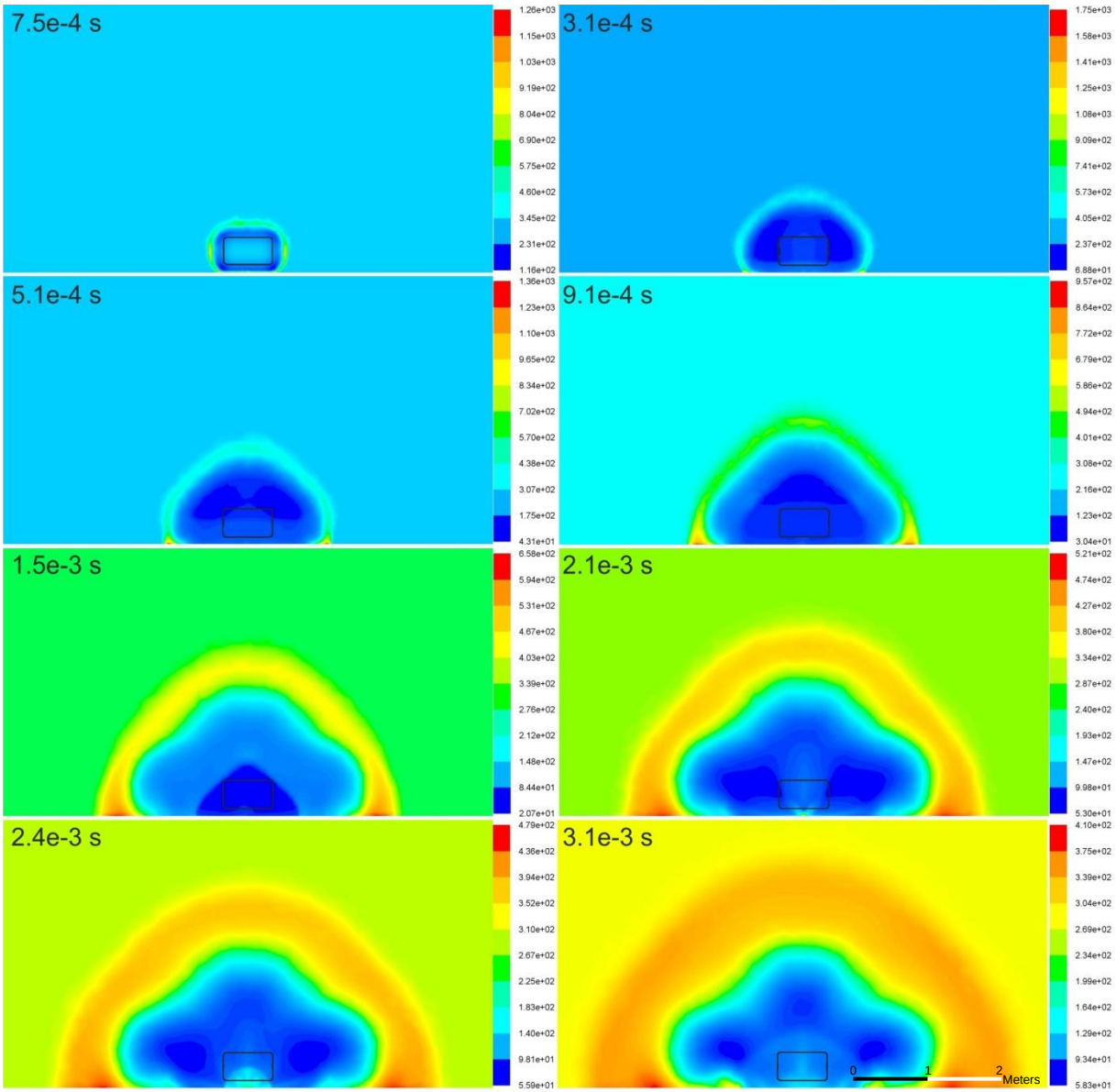

Figure 3. Temperature in the surroundings of the tank due to the rupture of the high pressure hydrogen tank

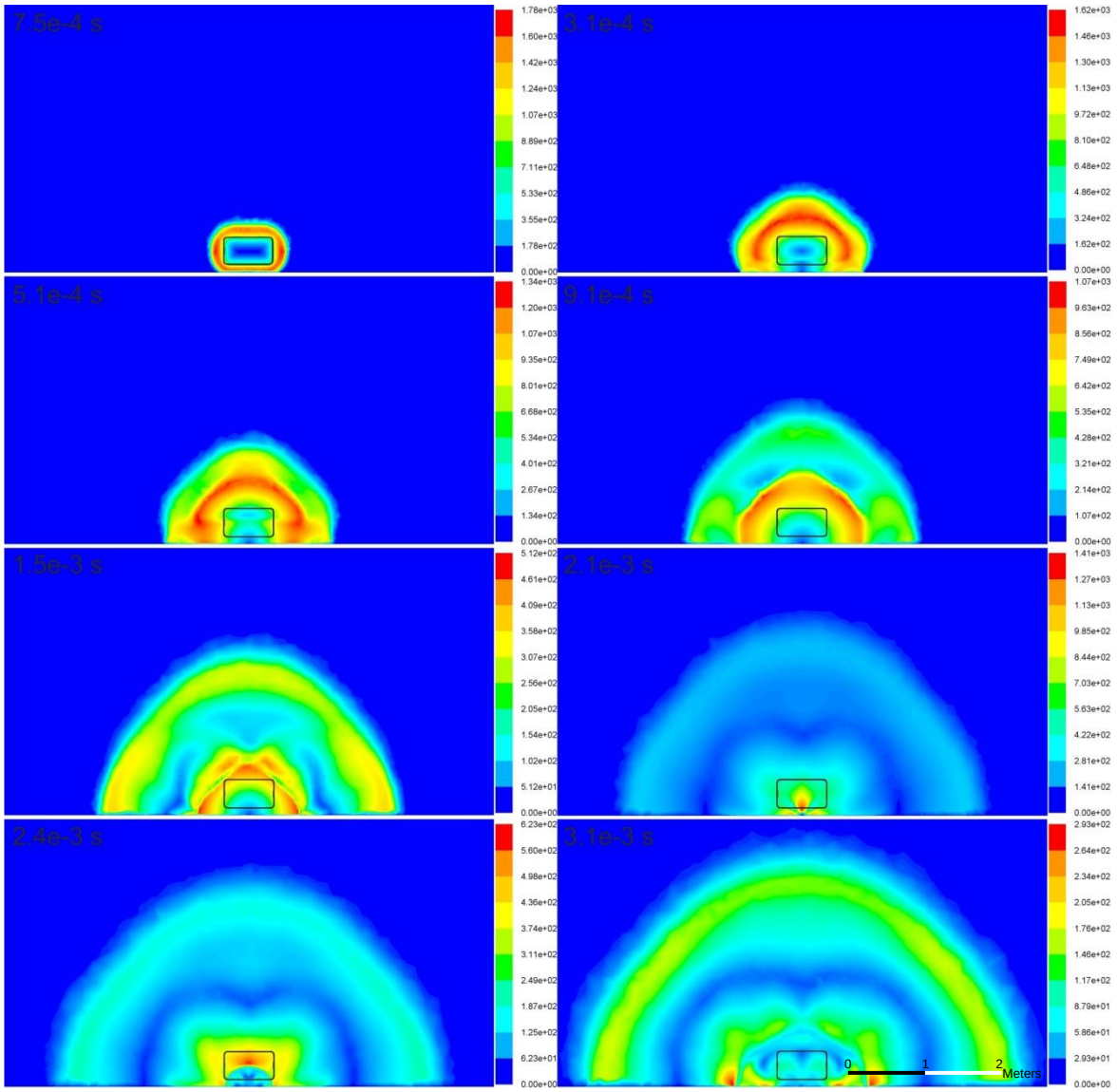

Figure 4. Velocity magnitude in the surroundings of the tank due to the rupture of the high pressure hydrogen tank

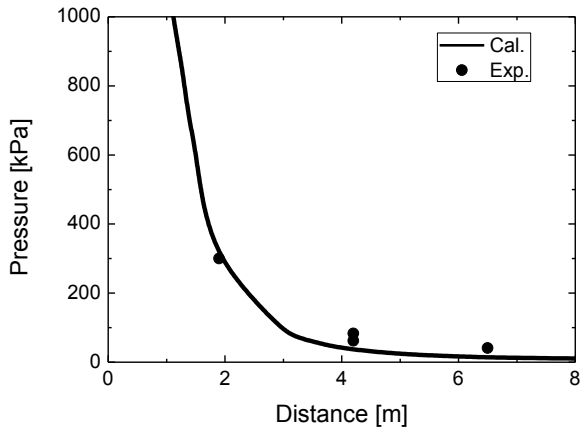

Figure 5. Comparison between experimental and numerical overpressure versus distances

4.2 Fireball

After the blast wave generation, the fireball formed upon the cylinder rupture. Because of the heat released by combustion and the buoyancy force, the fireball lifts off the ground and establishes a hemispherical cloud. The surrounding air mixes with hydrogen cloud due to intensive convection and diffusion processes and the hydrogen/air mixture in the cloud burns continuously as the remaining fuel mixes with the surrounding air. Figure 6 shows the hydrogen mass fraction in the fireball. As it was mentioned before, combustion practically does not have an effect on initial stage of rapid hydrogen expansion, t=0-5.1×10^{-3} s, and starts to play a noticeable role much later at approximately t=5.0×10^{-3} s. Hydrogen concentration starts to decrease due to combustion, in the first place - in the area of intensive hydrogen-air mixing (at hydrogen-air interface), remaining intact at the ground, see t=0.1-0.3 s in Figure 6. Once the hydrogen cloud is affected by buoyancy forces, mixing with air and combustion starts to take effect close to the ground too, t=0.3-0.5 s. The hydrogen cloud forms, then a shape characteristic for thermal plumes and attached to the ground by a narrow "stock", t=0.5-0.8 s, which then completely burnt and the mushroom-shaped cloud continues to burn in air, t=1.0-1.2 s.

Figures 7 and 8 show the temperature and the mass fraction of water vapour in the fireball cross-section. In simulations the flame is ignited closer to the ground where the largest generation of turbulence exists, giving rise to the combustion rate in equations (7)-(8) (while in the experiment the source of ignition should be, apparently, the bonfire burner). The flame propagates to the area of unburned hydrogen at the centre of the tank. Then, the flame has a more spherical shape at 0.8s, and it has lifted off the ground at 1.2 s after the rupture. The temperature of fireball on the ground increases to T=2540 K at t=0.3 s, and the fireball becomes hemispherical, which appears like a characteristic mushroom shape in cross-section.

The calculated maximum diameter of the fireball is 5.3 m at 1.0 s, which is somewhat below the size reported in experiment - 7.7 m [4]. Experimental images [4] suggest that the inhomogeneous luminosity of fireball is caused probably by the combustion of tank debris - polyethylene decomposition products and fragments of carbon fibers besides the hydrogen fuel. Presumably, the different fuels affect sharply varying luminosity of observed flame, which may be the reason for the larger visible fireball size reported in the experiments.

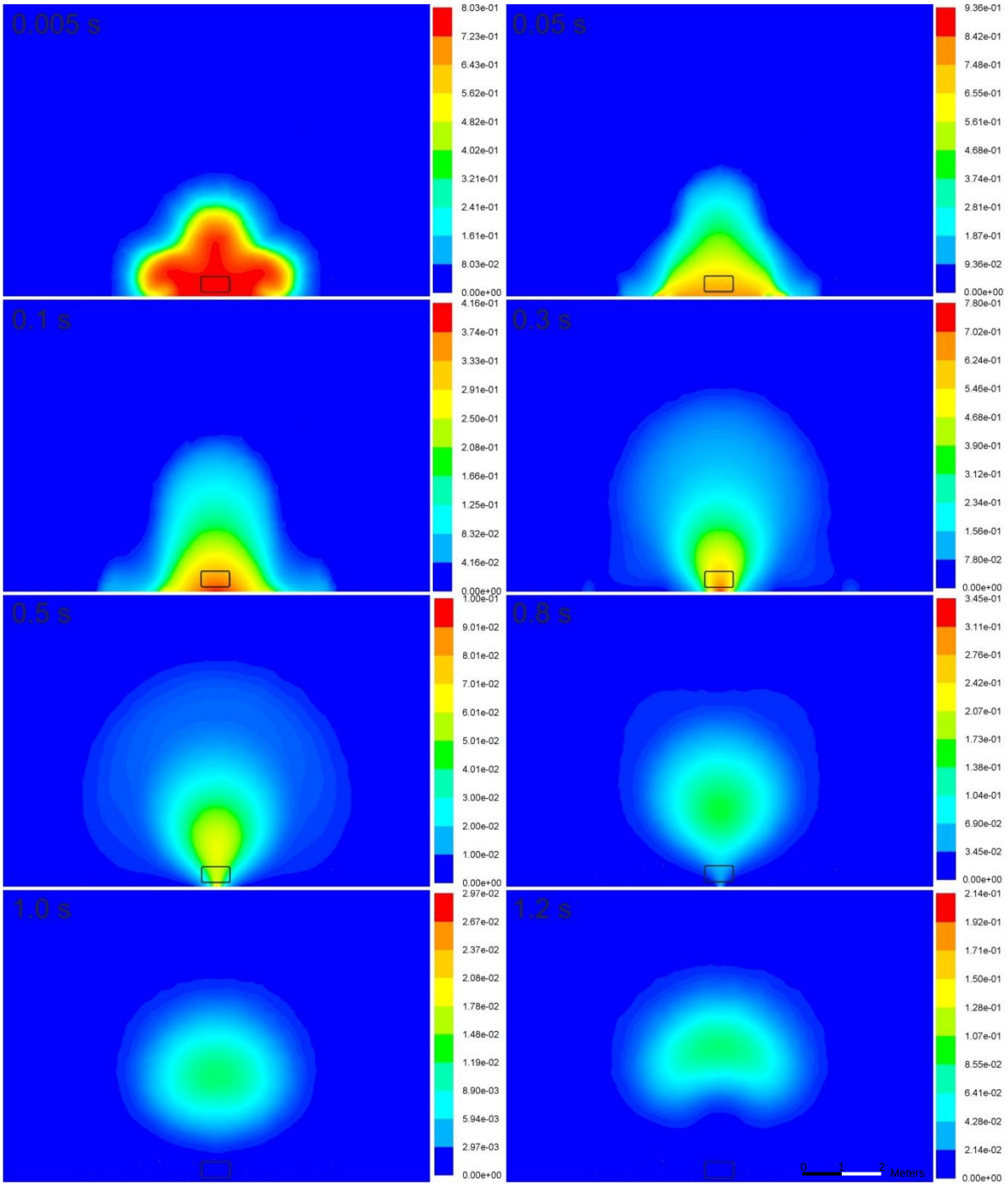

Figure 6. Mass fraction of hydrogen in the fireball cross-section.

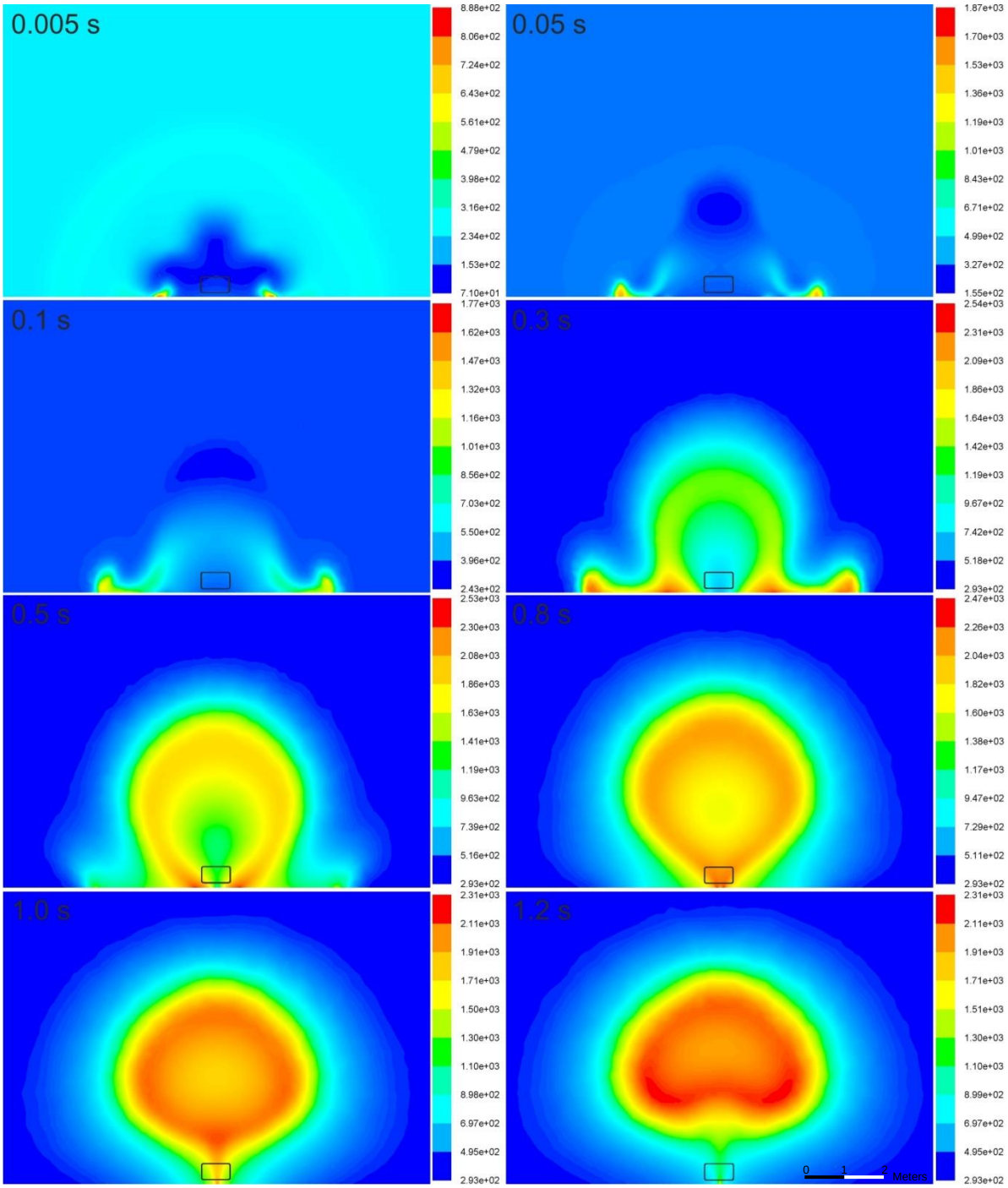

Figure 7. Temperature in the fireball cross section

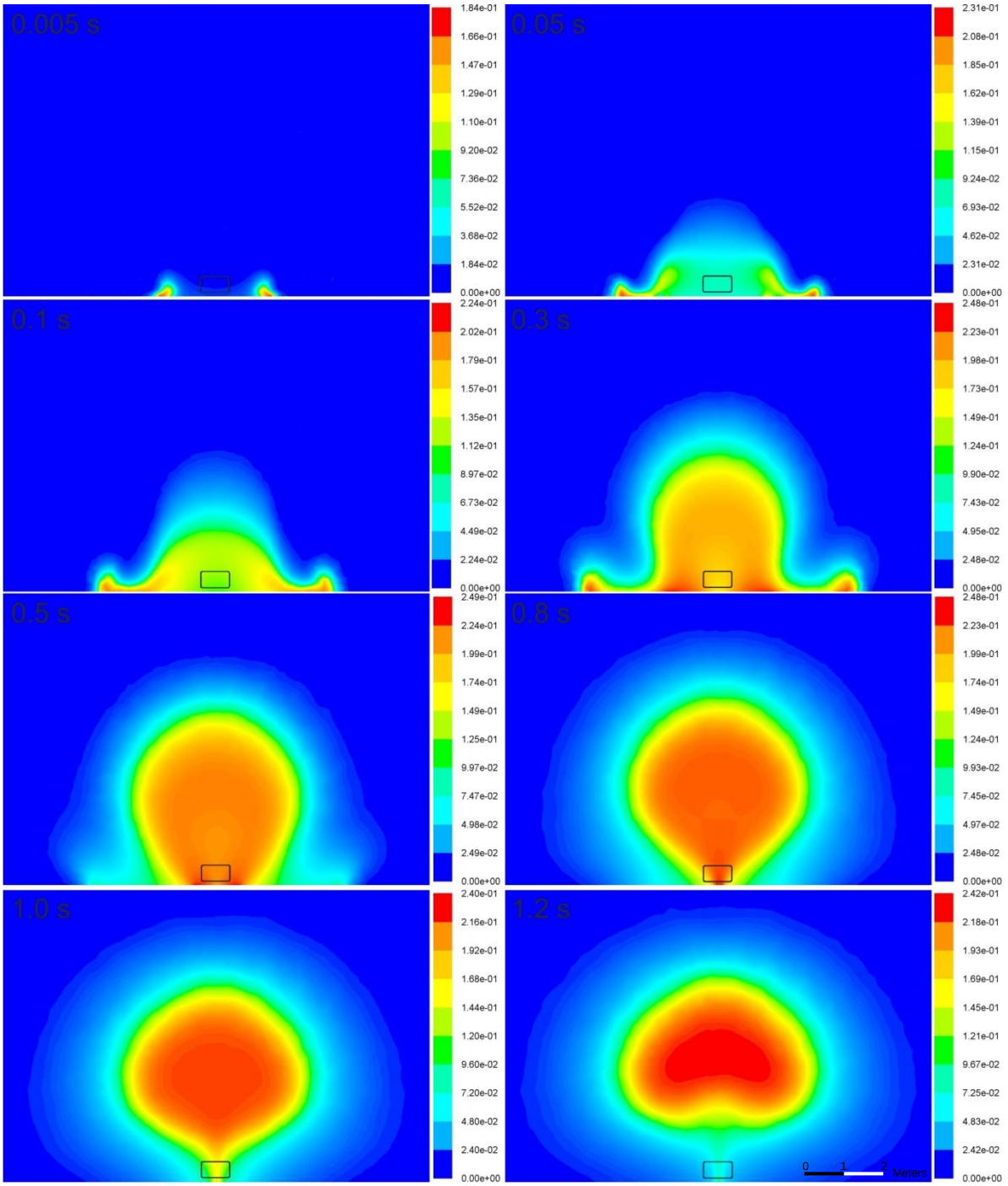

Figure 8. Mass fraction of water vapour in the fireball cross-section

5.0 CONCLUSIONS

The blast wave and fireball formed upon the high pressure (35 MPa) hydrogen tank (72 *l*) rupture have been investigated numerically. In the presented simulation the realizable *k-ε* turbulence model and the eddy dissipation model were applied to model turbulence and combustion respectively.

The simulation results are feasible and demonstrate close agreement with experimental observations. Simulated blast wave has generally a hemispherical shape, with blast overpressure quickly decreasing

due to radial expansion. Secondary pressure waves were reproduced in the simulations, resulting from pressure reflection from the ground and travelling through the expanding hydrogen cloud back and forth between ground and hydrogen-air interface. Combustion has negligible effect at the initial stage of hydrogen expansion and maximum temperature is due to adiabatic air compression, reaching T=1750 K at t=3.1×10^{-4} s. Hydrogen cloud expansion is affected by hydrogen tank shape with preferential expansion directions along main and transversal tank axes.

The simulation results of fireball indicate that blast wave and combustion develop practically independent, not interacting with each other with combustion taking place practically after hydrogen expansion is complete. In simulations the flame was ignited close to the ground and then propagated along hydrogen-air mixing interface, consuming hydrogen from the periphery to the centre of the cloud. The flame becomes a spherical shape at 0.8s, and it has lifted off the ground at 1.2s.

The calculated overpressure and fireball are compared with the results of the fire exposure tests of a stand-alone cylindrical hydrogen tank. Although the calculated overpressure at 1.9 m agrees with the measured overpressure, the calculated values at 4.2 m and 6.5 m are underestimated. In addition, the calculated maximum diameter of the fireball is 5.0 m at 1.0 s although the measured fireball size is about 7.7m. A potential reason for the difference between the experiments and the simulation results is that the measured value in the experiments is affected by the different fuels such as polyethylene decomposition products and fragments of carbon fibers, which combustion and luminosity are not accounted in simulations.

REFERENCES

1. Weyandt, N., Analysis of Induced Catastrophic Failure of a 5000 psig Type IV Hydrogen Cylinder, Southwest Research Institute Report 01.0639.01.001, February 2005.

2. Weyandt, N., Catastrophic Failure of a 5,000-psig Hydrogen Cylinder Installed on a Typical SUV, Southwest Research Institute Report 01.06939.01.005, November 2006.

3. Zalosh, R., and Weyandt, N., 2005. Hydrogen fuel tank fire exposure burst test. SAE Paper. 2005-01-1886.

4. Makarov, D., and Molkov, V., Plane hydrogen jets, *International Journal of Hydrogen Energy*, 38, 2013, pp. 8068-8083.

5. Shih, T.H., Liou, W.W., Shabbir, A., Yang, Z., and Zhu, J., A New Eddy-Viscosity Model for High Reynolds Number Turbulent Flows - Model Development and Validation, *Computers Fluids*. 24, 1995, pp. 227-238.

6. Magnussen, B.F. and Hjertager, B.H., On the Mathematical Modelling of Turbulent Combustion with Special Emphasis on Soot Formation and Combustion, 16th Symp. (Int.) on Combustion, Pittsburgh, PA, The Combustion Inst., 1976, pp. 711-729.

7. ANSYS Inc, 2009. ANSYS CFX. User's guide.

8. Zheng, J., Bie, H., Xu, P., Liu, P., Zhao, Y., Chen, H., Liu, X., and Zhao, L., Numerical simulation of high-pressure hydrogen jet flames during bonfire test, *International Journal of Hydrogen Energy*, 37, 2012, pp. 783-790.